Journal of Molecular Spectroscopy 399 (2024) 111873

Contents lists available at ScienceDirect

Journal of Molecular Spectroscopy

journal homepage: www.elsevier.com/locate/yjmsp

A spectroscopic investigation of the lowest electronic states of the I_2^+ cation as a candidate for detecting the time variation of fundamental constants

Yujie Zhao [a], Yali Tian [a], Xiaohu He [a], Ting Gong [a], Xiaocong Sun [a], Guqing Guo [a], Xuanbing Qiu [a], Xiang Yuan [b,c,*], Jinjun Liu [d,e,*], Lunhua Deng [f], Chuanliang Li [a,*]

[a] Shanxi Province Engineering Research Center of Precision Measurement and Online Detection Equipment, Shanxi Center of Technology Innovation for Light Manipulations and Applications, School of Applied Science, Taiyuan University of Science and Technology, Taiyuan 030024, China
[b] Université de Lille, CNRS, UMR 8523 - PhLAM - Physique des Lasers, Atomes et Molécules, F-59000 Lille, France
[c] Department of Chemistry and Pharmaceutical Science, Faculty of Science, Vrije Universiteit Amsterdam, de Boelelaan 1083, 1081 HV Amsterdam, The Netherlands
[d] Department of Chemistry, University of Louisville, Louisville, KY 40292, USA
[e] Department of Physics, University of Louisville, Louisville, KY 40292, USA
[f] State Key Laboratory of Precision Spectroscopy, East China Normal University, Shanghai 200062, China

ARTICLE INFO

Keywords:
I^+_2
Ab initio calculation
Radiative lifetime
Enhancement factors

ABSTRACT

The four lowest Ω substates ($X^2\Pi_{3/2,g}$, $X^2\Pi_{1/2,g}$, $A^2\Pi_{3/2,u}$ and $A^2\Pi_{1/2,u}$) of the I_2^+ cation have been studied by high-precision *ab initio* calculations in comparison with experimental high-resolution absorption spectra. The potential energy curves were calculated using the multi-reference configuration interaction (MRCI) method and Dirac method, respectively. Rovibrational levels of these electronic states were derived by solving the radial Schrödinger rovibrational equation. Molecular constants were obtained in fitting energy levels to a spectroscopic model. Using the fit spectroscopic constants and newly calculated transition dipole moment matrix elements, line strengths of vibronic bands in the $A^2\Pi_{3/2,u}$- $X^2\Pi_{3/2,g}$ system, as well as Einstein *A* coefficients for 45 of these bands with $\nu' = 11$–19 and $\nu'' = 1$–5, have been derived. The Einstein *A* coefficients were used to compute radiative lifetimes of the $\nu' = 11$–19 vibrational levels of the $A^2\Pi_{3/2,u}$ state. Enhancement factors for detecting the variation of the fine-structure constant (α) and the proton-to-electron mass ratio(μ) using transitions between nearly degenerate rovibronic levels of these low-lying states have been calculated.

1. Introduction

The cation of molecular iodine (I_2^+) has significant importance in the field of precision measurement due to its dense spectrum in a broad spectral range. Like other dihalogen cations, I_2^+ is also a promising candidate for detecting temporal and spatial variations of fundamental constants [1–6]. In search of strong enhancement effects of fundamental constant changes beyond the Standard Model, Pašteka *et al.*[7] investigated forbidden rotational vibrational transitions between the nearly degenerate sublevels of the $X^2\Pi$ ground state of cations of hydrogen halides and dihalides, examining the dependence of the transition energies on α and μ. Reliable candidate molecules are provided for future high-resolution experiments. Compared to other candidate molecules, the selected transitions in I_2^+ are particularly sensitive to the variation of α and μ due to its large spin–orbit (SO) splitting. In the present paper, we report a new computational investigation of rovibrational levels of the four lowest Ω substates ($X^2\Pi_{3/2,g}$, $X^2\Pi_{1/2,g}$, $A^2\Pi_{3/2,u}$ and $A^2\Pi_{1/2,u}$) of the I_2^+ cation. The computational results are benchmarked by experimental high-resolution optical heterodyne velocity modulation spectra of I_2^+. The spectrum simulated using calculated molecular constants well reproduced the experimental one, verifying our calculations. The enhancement factors for detecting the variation of α and μ are calculated using molecular constants and energy levels obtained in the present work.

Early spectroscopic data of I_2^+ were mainly derived from experimental measurements with vibrational resolution. Photoelectron spectroscopy (PES) technology was first used to study the vibrational structure of the electronic states of I_2^+ [8]. Low-resolution spectra providing information of the $X^2\Pi_g$ and $A^2\Pi_u$ states of I_2^+ were observed in the HeI PES experiment [8–11]. In 1973, vibrationally resolved

* Corresponding authors at: Université de Lille, CNRS, UMR 8523 - PhLAM - Physique des Lasers, Atomes et Molécules, F-59000 Lille, France (X. Yuan). Department of Chemistry, University of Louisville, Louisville, KY 40292, USA (J. Liu).
E-mail addresses: xiang.yuan@univ-lille.fr (X. Yuan), j.liu@louisville.edu (J. Liu), clli@tyust.edu.cn (C. Li).

https://doi.org/10.1016/j.jms.2023.111873
Received 4 September 2023; Received in revised form 7 December 2023; Accepted 30 December 2023
Available online 2 January 2024

spectra of the I_2^+ cation were obtained in a NeI PES experiment, in which the first two adiabatic ionization potentials of the cation were determined [12]. In 1984, vibrational constants ω_e and $\omega_e\chi_e$ of the $X^2\Pi_g$ state of I_2^+ were determined by fitting spectra obtained using the H Lyman α radiation UV PES technology [13]. The emission spectra of the $A^2\Pi_{3/2,u}$-$X^2\Pi_{3/2,g}$ system of I_2^+ were first observed in the same year [14]. Later Horner and Eland reported the measurement of the vibrationally resolved *A-X* emission spectrum in the region of 600–950 nm. In 1989, the $A^2\Pi_u$ - $X^2\Pi_g$ electronic emission spectrum of I_2^+ in the range of 620–800 nm was recorded using the crossed molecular beam/electron beam technique at a lower rotational temperature by Mason and Tuckett [15]. In 1994, Yencha *et al.* measured the threshold photoelectron spectrum of I_2, which revealed the vibrational structure in each SO component of $X^2\Pi_g$ [16]. They also determined the averaged vibrational spacings of $A^2\Pi_u$. However, a full vibrational analysis was not attempted due to low spectral resolution.

During the mid-1990s, high-resolution pulsed-field ionization zero-kinetic-energy (PFI-ZEKE) photoelectron spectroscopy was used to study the electronic states of I_2^+ [17–19]. Cockett *et al.* employed a (2 + 1′) resonance-enhanced multiphoton ionization (REMPI) scheme with intermediate Rydberg states, and obtained the values for ω_e and $\omega_e\chi_e$ of the $X^2\Pi_g$ state [17]. Later, they observed widely extended vibrational progressions using the $B^3\Pi_0$ state as the intermediate state in a (1 + 2′) scheme and re-determined the values of ω_e and $\omega_e\chi_e$ of the $X^2\Pi_g$ state [18]. Furthermore, they observed the vibrational structures of the first electronically excited state ($A^2\Pi_{3/2,u}$) and a new electronic state ($a^4\Sigma^-_u$) of I_2^+ for the first time [19]. In 2012, Deng *et al.* reported rotationally resolved absorption spectra of I_2^+ in the 12,065–13,062 cm^{-1} region by using the optical heterodyne velocity modulation spectroscopy [20]. The spectral region for I_2^+ study was further extended to 11,860–12,060 cm^{-1} in 2017 [21].

Theoretical calculations have been carried out to study the electronic states of I_2^+. In 1989, spectroscopic parameters (T_e, r_e, ω_e, *etc.*) of 13 electronic states of I_2^+ were derived using the large-scale multi-configuration self-consistent field/configuration interaction (MCSCF/CI) method by Li and Balasubramanian [22]. Later low-lying electronic states of I_2^+ were calculated using the Four-component relativistic coupled-cluster by de Jong *et al.* [23]. They also predicted the potential energies of I_2^+ using the complete open-shell configuration interaction approach. However, the accuracy of theoretical calculations is limited by the strong relativistic effect of iodine and the complex electronic structure of I_2^+. From an experimental point of view, spectra of I_2^+ are often contaminated by the neutral I_2 molecule, leading to difficulties in the spectral assignment.

In this paper, the potential energy curves (PECs) of $X^2\Pi_{3/2,g}$, $X^2\Pi_{1/2,g}$, $A^2\Pi_{3/2,u}$, and $A^2\Pi_{1/2,u}$ states of I_2^+ are calculated using high-precision *ab initio* methods. The spectroscopic parameters determined for these states are compared with previous theoretical and experimental results. The calculations of the Einstein *A* coefficients and relative line strengths for the $A^2\Pi_{3/2,u}$- $X^2\Pi_{3/2,g}$ system of I_2^+ are also reported. Transition dipole moments (TDMs) determined in the present work are used to predict transition intensities. Finally, following the approaches of Pašteka *et al.* [7], we identified nearly degenerate rovibronic levels in the $X^2\Pi_{1/2,g}$- $X^2\Pi_{3/2,g}$ system that can be utilized in the search for the variation of α and μ, and calculated the enhancement factors for transitions between these level pairs. In the present work, rovibrational structures of both SO components of the ground electronic state have been calculated. Therefore, the present work provides a more reliable identification of nearly degenerate states for future experiments and a more accurate prediction of the enhancement factors.

2. Methods of calculations

2.1. Potential energy curves and rovibrational energy levels

The *ab initio* calculations were performed using the MOLPRO 2012 software package [25,26], in which the point group for a homonuclear diatomic is reduced from $D_{\infty h}$ to D_{2h}. The PECs calculations were carried out with a step size of 0.02 Å near the minima of the $X^2\Pi$ and $A^2\Pi$ states. Larger step sizes were used in other regions (with internuclear distance ranging from 2 to 6.5 Å). For the basis set, the cc-pwCVTZ-PP basis set [27] is adopted for iodine.

The current electronic structure calculations consist of three steps: First the single configuration wave-function is computed by Hartree-Fock method. Subsequently, the molecular orbitals are optimized by the state-averaged complete active space selfconsistent field (SA-CASSCF) [28] method. Finally, based on the orbitals from the SA-CASSCF calculations, the internally contracted multi-reference configuration interaction (MRCI) [29] calculations is performed to take account of electronic dynamic correlation. In the SA-CASSCF calculation, the active space consists of eight molecular orbitals: two a_g, one b_{3u}, one b_{2u}, two b_{1u}, one b_{2g}, and one b_{3g}, which associated with the 5s and 5p orbitals of I. For heavy element calculations like iodine, it is necessary to consider the core-valence effect, which is mainly from semi-core shell electrons. Therefore, in addition to the valence orbitals, the 4s, 4p, and 4d semi-core orbitals of iodine were also correlated in the MRCI calculation.

The SO coupling is considered as a perturbation and is evaluated with the state-interacting method, in which the spin–orbit states were obtained by the diagonalization of the whole spin–orbit Hamiltonian on the basis of spin-free states. Apart from the PECs, the electronic TDMs of the $A^2\Pi_{3/2,u}$ - $X^2\Pi_{3/2,g}$ system were also determined in the current MRCI calculations.

As it is found in the literature [30–32], the calculations of SO coupling based on perturbation theory can be very sensitive to the number of electronic spin-free states entering the CI calculation. To benchmark the SO coupling effect and cross-validate the MRCI result, calculations of ionization potential with the relativistic equation-of-motion coupled-cluster single and double (EOM-CCSD-IP) [33] have also carried out, in which the SO coupling being accounted for by a variational method based upon a four-component Hamiltonian.

In the EOM-CCSD-IP calculation, the ground state CCSD equation of the neutral molecule I_2 obtained the T_1 and T_2 amplitudes [34]. Utilizing T_1 and T_2, the similar-transformed Hamiltonian matrix $\overline{H}$ constructed and iteratively diagonalized it to determine the ionization energy. All the calculations are performed with the relativistic quantum chemistry package DIRAC19 [35,36]. The Hamiltonian used in the EOM-CCSD-IP is the four-component Dirac-Coulomb (DC) Hamiltonian with the approximation of the (SS|SS) integrals by a Coulombic correction [37]. Uncontracted Dyall basis sets, specifically v3z [38], are adopted for iodine. Since EOM-CCSD is a single-reference method, we scan the PECs of $X^2\Pi_{3/2,g}$, $X^2\Pi_{1/2,g}$, $A^2\Pi_{3/2,u}$, and $A^2\Pi_{1/2,u}$ four substates in the bound region from 2.2 Å to 3.6 Å.

Based on the PECs, the vibrational wave functions and rovibrational energy levels were obtained by solving the one-dimensional radial Schrödinger equation of diatomic molecules using the LEVEL program [39]. Finally, molecular constants of the $X^2\Pi_{3/2,g}$, $X^2\Pi_{1/2,g}$, $A^2\Pi_{3/2,u}$, and $A^2\Pi_{1/2,u}$ substates, including the harmonic frequency ω_e, the first-order anharmonic coefficient $\omega_e\chi_e$, and the rotational constant B_e at the equilibrium internuclear distance R_e, were determined in a nonlinear least-squares fitting of the rovibrational energy levels.

2.2. Line strengths and Einstein a constants

The line strength of a transition between different rovibrational levels of two electronic states $S_{v',v'',J',J''}$ is proportional to the square of the corresponding (rotation-free) TDM matrix element [40,41]:

$$S_{v',v'',J',J''} \propto \int \psi^{*}_{v',J'}(R)\Re_e(R)\psi_{v'',J''}dR \quad (1)$$

where R is the internuclear distance, $\Psi_{v'',J''}(R)$ and $\Psi_{v',J'}(R)$ are rovibronic wave functions of the ground and excited states, respectively, and $\Re_e(R)$ is the (electronic) TDM. which can be calculated using the following equation:

$$\Re_e(R) = \int \psi^{'*}_{el}(R, r_i)\mu(R, r_i)\psi^{''}_{el}(R, r_i)d\tau_{el} \quad (2)$$

where r_i's are electron coordinates, Ψ_{el} (R, r_i)'s are electronic wave functions, and $\mu(R, r_i)$ is the electric dipole moment operator. The integration is over all electron coordinates. The effective potential energy function (V_{effect}) can be used to obtain the vibrational wave functions in Eq. (1). V_{effect} can be derived using the Rydberg Klein-Rees (RKR) method [40] or solely from *ab initio* calculations. In the present work, the effective potential energy functions for the $A^2\Pi_{3/2,u}$ and $X^2\Pi_{3/2,g}$ states were constructed using the RKR1 program [42] with the equilibrium spectroscopic constants provided in Ref. [21]. The RKR potentials of the two lower Ω substates ($A^2\Pi_{3/2,u}$ and $X^2\Pi_{3/2,g}$) and the electronic TDMs from high-precision *ab initio* calculations were then used in LEVEL to produce the TDM matrix elements using Eq. (2). The Hönl-London factors were generated in the PGOPHER program and combined with the rotational-free TDM matrix elements (see above).

Einstein A coefficients were obtained in the PGOPHER program [43] using the following expression:

$$A_{v',J'\to v'',J''} = 3.13618932 \times 10^{-7}\nu^3\frac{S_{v',v'',J',J''}}{(2J'+1)} \quad (3)$$

where the line strength $S_{v',v'',J',J''}$ (in the unit of debye squared) is summed over the degenerate M components of both upper and lower states:

$$S_{v',v'',J',J''} = \sum_{M',M''}\left|\left\langle\psi_{v',J'M'}(R)\middle|\Re e(R)\middle|\psi_{v'',J''M''}(R)\right\rangle\right|^2 \quad (4)$$

The radiative lifetime of a rovibrational level of excited electronic states was calculated as the reciprocal of the sum of Einstein A coefficients for all possible (downward) transitions from this level.

3. Results and discussion

3.1. Potential energy curves and spectroscopic properties of Ω substates

Our calculations include 24 Λ-S electronic states of I_2^+ (two $^{2,4}\Pi_g$,two $^{2,4}\Pi_u$, one $^{2,4}\Sigma^+_g$, one $^{2,4}\Sigma^+_u$, two $^{2,4}\Sigma^-_g$, two $^{2,4}\Sigma^-_u$, one $^{2,4}\Delta_g$, and one $^{2,4}\Delta_u$ states). These electronic states result from a combination of the ^3P_g ground state of I^+ and the ^2P_u ground state of I. Fig. 1a illustrates the calculated PECs of the doublet states correlated to the first asymptote (I^+ (^3P_g) + I (^2P_u)). The quartet states are not included for clarity. Equilibrium internuclear distances of the $X^2\Pi_g$ and $A^2\Pi_u$ states are 2.6 and 2.9 Å, respectively. At the equilibrium internuclear distance, the ground ($X^2\Pi_g$) state arises mainly (90.94 %) from the configuration of … $12\sigma_g^2 12\sigma_u^2 13\sigma_g^2 6\pi_u^4 6\pi_g^3$. The first excited ($A^2\Pi_u$) state is generated by the promotion of an electron from the $6\pi_u$ to the $6\pi_g$ orbital.

The SO interaction splits the $X^2\Pi_g$ state into $X^2\Pi_{3/2,g}$ and $X^2\Pi_{1/2,g}$ substates, and the $A^2\Pi_u$ state into $A^2\Pi_{3/2,u}$ and $A^2\Pi_{1/2,u}$ substates. In Fig. 1b the PECs of the four substates are displayed. For both the $X^2\Pi_g$ and $A^2\Pi_u$ states, the SO constants are negative. The $X^2\Pi_{1/2,g}$ and $A^2\Pi_{1/2,u}$ components are about 5842 cm^{-1} and 4740 cm^{-1} higher than their respective Ω = 3/2 counterparts at equilibria.

Spectroscopic parameters obtained in fitting the PECs are listed in Table 1 and compared with previously calculated and experimental results. Using the MOLPRO software, our calculated SO free T_e of the $A^2\Pi_u$ state, taken as the center of the two Ω substates, is 12,037 cm^{-1}, which is significantly higher than the value reported in Ref. [22], 9603 cm^{-1}. The X-state SO splitting we calculated (5482 cm^{-1}) is 497 cm^{-1} less than that from Li and Balasubramanian (5979 cm^{-1})[22], while our A-state value (4740 cm^{-1}) is 309 cm^{-1} less than the value they reported (5049 cm^{-1}). R_e, D_e, and ω_e of these four substates determined in the present work are not in good agreement with Ref. [22]. Our calculated values are closer to the experimental ones [22,23], which is attributed to the larger number of electronic states included in our calculations. R_e and ω_e values from this work are in good agreement with the results of de Jong *et al.* [23] except for ω_e of the $X^2\Pi_{3/2,g}$ state. Our ω_e values for the $X^2\Pi_{1/2,g}$ and $A^2\Pi_{3/2,u}$ states are consistent with the ones reported by Cockett *et al.* [19], whereas our values of $\omega_e\chi_e$ are significantly smaller than theirs. Our D_0's for $X^2\Pi_{3/2,g}$ and $X^2\Pi_{1/2,g}$ are about 1700 cm^{-1} and 2000 cm^{-1} less than the corresponding results in Ref. [19]. Deng *et al.* [20] determined the parameters of the $X^2\Pi_{3/2,g}$ and $A^2\Pi_{3/2,u}$ states in a high-resolution spectroscopy investigation (see below). For the $X^2\Pi_{3/2,g}$ state, the parameters R_e, B_e, α_e, and $\omega_e\chi_e$ determined in the present work are consistent with the values they reported, whereas discrepancy exists for ω_e. For the $A^2\Pi_{3/2,u}$ state, R_e, B_e and ω_e values from our calculations match nicely with those in Ref. [20], but the values of α_e and $\omega_e\chi_e$ differ.

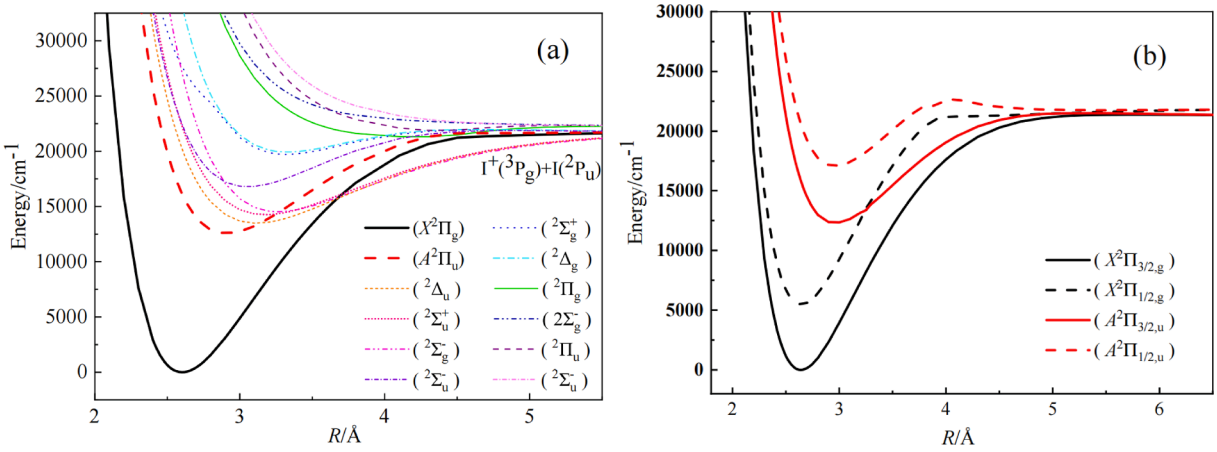

Fig. 1. (Color online) (a) PECs of the doublet states of I_2^+ correlated to the first asymptote. (b) PECs of the $X^2\Pi_g$ and $A^2\Pi_u$ states in the presence of the SO interaction.

Table 1
Spectroscopic constants of the lowest four Ω substates of I_2^+.

State	Ref.	Te (cm^{-1})	Re(Å)	Be (cm^{-1})	De(eV)	αe (cm^{-1})	ωe (cm^{-1})	ωeχe(cm^{-1})	D0 (cm^{-1})
*X*2Π3/2,g	This work with MOLPRO	0	2.637	0.038	2.49	1.05×10^{-4}	230.9	0.58	19982.37
	This work with DIRAC	0	2.600	0.039	1.84	1.10×10^{-4}	243.0	0.64	
	Cal. [22]	0	2.69		2.06		217		
	Cal. [23]		2.613				238		
	Exp. [19]						240(1)	0.71(1)	21679(3)
	Exp. [20]		2.584	0.039		1.18×10^{-4}	239.0	0.65	
*X*2Π1/2,g	This work with MOLPRO	5482	2.628	0.038	1.81	1.47×10^{-4}	232.4	0.46	14501.25
	This work with DIRAC	5153	2.601	0.039	1.58	1.06×10^{-4}	233.7	0.69	
	Cal. [22]	5979	2.69		1.3		208		
	Cal. [23]		2.626				227		
	Exp. [19]						229(2)	0.75(4)	16482(3)
	Exp. [24]	5180							
*A*2Π3/2,u	This work with MOLPRO	12,408	2.930	0.031	0.955	3.13×10^{-4}	139.1	0.81	7635.69
	This work with DIRAC	13,660	2.903	0.031	0.543	1.14×10^{-4}	156.2	0.58	
	Cal. [22]	10,068	3.09				132		
	Cal. [23]		2.949				140		
	Exp. [19]						138(2)	0.46(1)	10381(3)
	Exp. [20]		2.947(1)	0.031		1.24×10^{-4}	138.1	0.45	
*A*2Π1/2,u	This work with MOLPRO	17,148	2.928	0.031	0.368	7.33×10^{-4}	151.5	2.64	2890.06
	This work with DIRAC	19,476	2.875	0.032	0.680	1.30×10^{-4}	167.9	0.54	
	Cal. [22]	15,117	3.11				112		
	Cal. [23]		2.91				156		

Using the DIRAC software, the *X*-state split (5153 cm^{-1}) calculated is 826 cm^{-1} lower than that in reference [22] (5979 cm^{-1}), but the *A*-state value (5979 cm^{-1}) is 930 cm^{-1} higher than the value they reported (5049 cm^{-1}). The spectral parameters of ground state *X*-states are in good agreement with the experimental values. The $X^2\Pi_{3/2,g}$ state is highly consistent with the experiment values [20]. The differences between the calculated R_e, B_e, ω_e, $\omega_e\chi_e$ and the experimental values [20] are only 0.0152 Å, 0.00056 cm^{-1}, 3.9413 cm^{-1} and 0.005 cm^{-1}. The calculated ω_e and $\omega_e\chi_e$ values of the $A^2\Pi_{1/2,g}$ state are closer to the experimental value [19], where ω_e is 4.715 cm^{-1} higher than the experimental value, and $\omega_e\chi_e$ differs 0.06 cm^{-1} from the value 0.75 cm^{-1}. The calculated T_e differs from the experimental value [24] by merely 27 cm^{-1}. B_e, α_e of *A*-state are in better agreement with theoretical and experimental values [20]. However, R_e, ω_e, $\omega_e\chi_e$ are slightly different [22]. The comparison reveals that the vibrational constants are closer to the data in the theoretical literature [23].

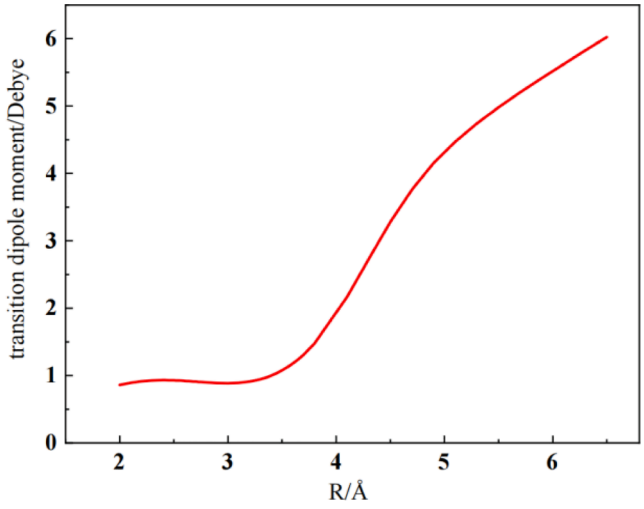

Fig. 2. (Color online) Electronic TDM of the $A^2\Pi_{3/2,u}$ - $X^2\Pi_{3/2,g}$ system as a function of the internuclear distance (*R*).

3.2. Line strengths and lifetimes

The calculated electronic TDM function for the $A^2\Pi_{3/2,u} \leftarrow X^2\Pi_{3/2,g}$ transition as a function of the internuclear distance is illustrated in Fig. 2. It was used to generate the TDM matrices for different vibronic bands, which were used to calculate the Einstein *A* coefficients for rovibronic transitions and lifetimes of $v' = 11$–19 vibronic levels of the $A^2\Pi_{3/2,u}$ state. Our computed values for lifetimes are listed in Table 2. To the best of our knowledge, no experimental values of lifetimes of electronic states of I_2^+ have been reported.

3.3. Simulation and fitting of the experimental spectrum

To benchmark our calculations, the rotationally resolved optical heterodyne velocity modulation spectrum of the $A^2\Pi_{3/2,u}$-$X^2\Pi_{3/2,g}$ system of I_2^+ [20] was simulated using the calculated molecular constants and the electronic TDM function. The lineshapes of the experimental spectrum can be well reproduced using the second derivative of a Voigt lineshape. The Lorentzian and Gaussian linewidths were set to 0.019 and 0.026 cm^{-1}, respectively, in the calculated spectrum to match the experimental lineshapes. A rotational temperature of ~ 340 K and a vibrational temperature of ~ 1500 K were determined in reproducing the relative transition intensities.

The simulated spectrum of the $A^2\Pi_{3/2,u}$ - $X^2\Pi_{3/2,g}$ system of I_2^+ in the region of 12,681–13,037 cm^{-1} is compared with the experimentally obtained one in Fig. 3, which includes mainly transitions of the (13,1), (15,2), (14,1), (17,3), (16,2), (15,1), (18,3), (17,2), and (19,3) bands. The overall intensity pattern of the simulated spectrum is close to the observed one. However, transition intensities of the simulated spectrum are in general weaker than the experimental one in the range of 12,920–13,037 cm^{-1}, dominated by the (17,2) band. The discrepancy is attributed to the unsatisfactory laser stability in this high-frequency region approaching the blue-limit of the Ti: Sapphire laser source. An excellent match between the simulated and experimental transition intensities is found in other covered regions. A detailed comparison in the region of 12,781.25–12,788.17 cm^{-1} is illustrated in Fig. 4, which demonstrates the quality of the simulation.

Table 2
Lifetimes of vibrational levels of the $A^2\Pi_{3/2,u}$ state of I_2^+.

v'	11	12	13	14	15	16	17	18	19
$\tau(\mu s)$	2.29	2.18	2.22	2.15	2.20	1.88	2.32	2.38	2.42

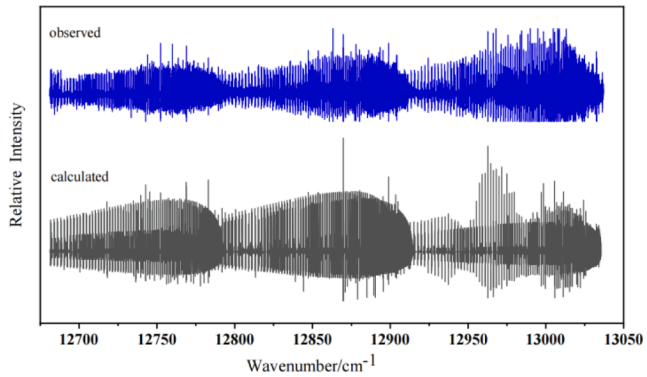

Fig. 3. (Color online) Comparison of the experimental (upper) and simulated (lower) spectra of I_2^+ in the region of 12,681 – 13,037 cm^{-1}.

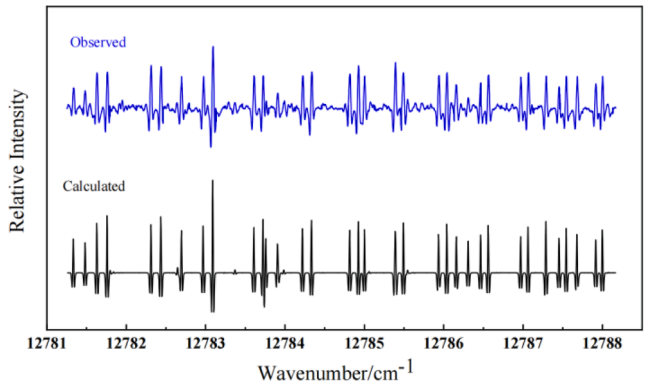

Fig. 4. (Color online) A detailed comparison of the experimental (upper) and simulated (lower) spectra in the region of 12,781.25–12,788.17 cm^{-1}.

4. Implications for detecting the variation of fundamental constants

Transition frequencies between rovibroic energy levels of the $X^2\Pi_{3/2,g}$ and $X^2\Pi_{1/2,g}$ substates can be calculated as [7]:

$$\begin{aligned}\omega &= E' - E'' \\ &= \omega_e(v' - v'') - \omega_e\chi_e(v' - v'')(v'' + v' + 1) \\ &\quad + B_e(J' - J'')(J'' + J' + 1) \\ &\quad - A_e - \frac{1}{2}A^{(1)}(v'' + v' + 1)\end{aligned} \tag{5}$$

where A_e and $A^{(1)}$ are the SO constant and its first vibrational correction, respectively. If the mass ratio between the proton and electron (μ) and the fine-structure constant (α) vary, the variation of the transition frequency ω can be expressed as:

$$\frac{\delta\omega}{\omega} = K_\mu\frac{\delta\mu}{\mu} + K_\alpha\frac{\delta\alpha}{\alpha} = \frac{\widetilde{K}_\mu}{\omega}\frac{\delta\mu}{\mu} + \frac{\widetilde{K}_\alpha}{\omega}\frac{\delta\alpha}{\alpha} \tag{6}$$

where K_μ and K_α are enhancement factors, $\widetilde{K}_\mu$ and $\widetilde{K}_\alpha$ are absolute enhancement factors, and $\delta\omega$ is the statistical uncertainty of ω assuming white noise, which can be calculated as [43]:

$$\delta\omega = \frac{\Gamma}{\sqrt{M}S/\delta S} \tag{7}$$

In Eq. (7) Γ is the linewidth, $S/\delta S$ is the signal-to-noise ratio of the spectroscopic measurement, and M is the number of independent measurements. From Eq. (5), the (absolute) enhancement factors for transitions between the $X^2\Pi_{3/2,g}$ and $X^2\Pi_{1/2,g}$ substates can be calculated as [7]:

$$\begin{aligned}K_\mu &= \Big(\frac{1}{2}\omega_e(v'' - v') - \omega_e\chi_e(v'' - v')(v'' + v' + 1) \\ &\quad + B_e(J'' - J')(J'' + J' + 1) \\ &\quad + \frac{1}{4}A^{(1)}(v'' + v' + 1)\omega^{-1}\Big) \\ &= \widetilde{K}_\mu\omega^{-1}\end{aligned} \tag{8}$$

And

$$K_\alpha = \big(-2A_e - A^{(1)}(v'' + v' + 1)\big)\omega^{-1} = \widetilde{K}_\alpha\omega^{-1} \tag{9}$$

As an example, the rovibrational energy levels of the two SO components of the $X^2\Pi_g$ electronic state of I_2^+ obtained from *ab initio* calculations are illustrated in Fig. 5. The v''= 45,52,59 energy levels of the $X^2\Pi_{3/2,g}$ state of I_2^+, obtained by *ab initio* calculation with MOLPRO, exhibit almost degeneracy with the v'= 17,23,29 energy levels of the $X^2\Pi_{1/2,g}$ state, respectively, and the energy separation is less than 0.4 cm^{-1}. The v''= 30,43,54 energy levels of $X^2\Pi_{3/2,g}$ state, calculated by Dirac, closely resemble degeneracy with the v'= 7,19,29 energy levels of $X^2\Pi_{1/2,g}$ state, respectively. A closer look at the rotational structure reveals that the near-degenerate vibrational levels of these two SO components have a smaller separation (See Fig. 6 (a) and (b)). The observed disparities in degeneracy patterns between the two program packages are duly noted. It is recognized that these differences indicate potential variations from actual levels. While the calculated molecular parameters align closely with the experimental values, except the T_e, particularly for the ones derived from the DIRAC methods. To enhance the predictive accuracy of rovibrational energy levels, we deduce predictions based on

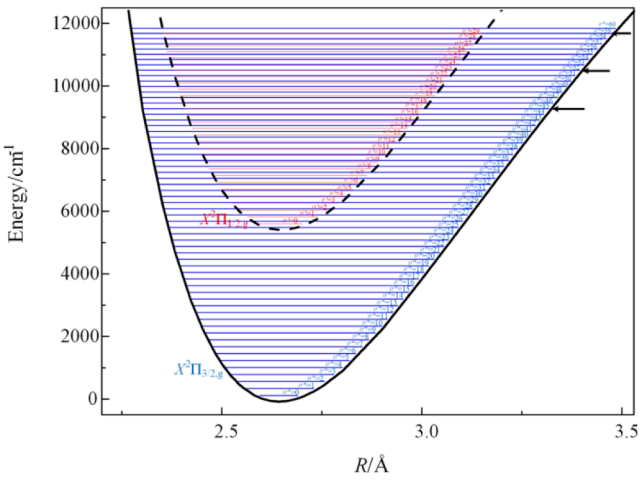

Fig. 5. (Color online) PECs of the two substates of I_2^+: $X^2\Pi_{3/2,g}$ (solid curve) and $X^2\Pi_{1/2,g}$ (dashed curve). Arrows point to the nearly degenerate vibrational levels of $X^2\Pi_{3/2,g}$ (blue lines) and $X^2\Pi_{1/2,g}$ (red lines).

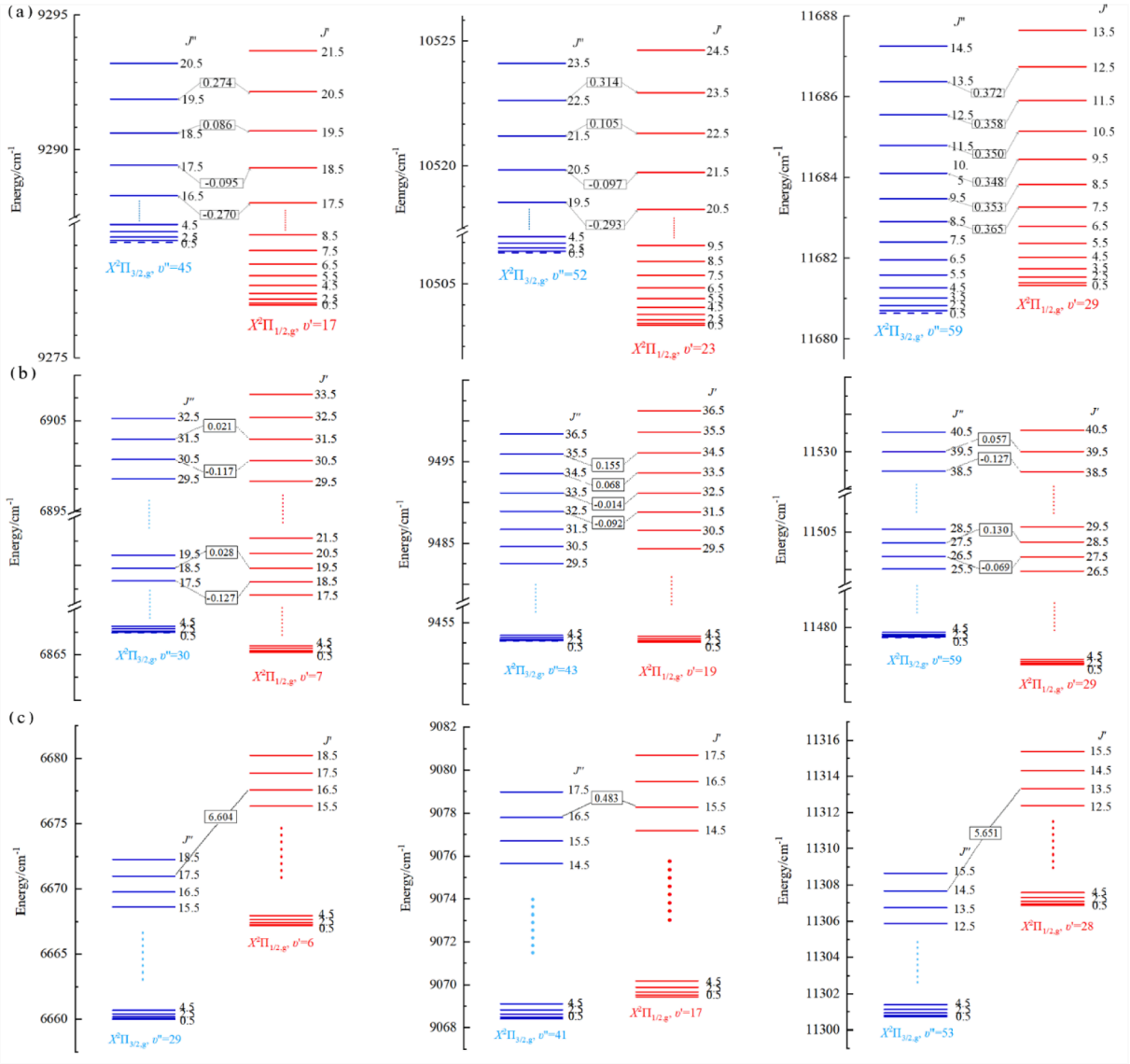

Fig. 6. (Color online) Rotational structure of the selected nearly degenerate vibrational levels of I_2^+ in its $X^2\Pi_{3/2,g}$ (blue lines) and $X^2\Pi_{1/2,g}$ (red lines) substates. Energy separations between nearly degenerate rotational levels are also indicated. (a) using the MOLPRO, (b) using the DIRAC, (c) using the experimental data obtained from T_e fitting.

the constants of DIRAC in combination with the experimental T_e, as plotted in Fig. 6 (c). Similarly, the $v''=29,41,53$ energy levels of $X^2\Pi_{3/2,g}$ state are closely degenerate with the $v'=6,17,28$ energy levels of $X^2\Pi_{1/2,g}$ state, with an energy separation of less than 6 cm^{-1}. These results demonstrate that the observed disparities can indeed serve as evidence for the existence of degeneracy, considering the high density of rovibrational energy levels and the large spin–orbit coupling splitting. Table 3 summarizes the almost degenerate pairs of energy levels obtained using MOLPRO and DIRAC, and the transition frequencies and (absolute) enhancement factors between them.

We now estimate the sensitivity of detecting the variation of μ and α using these nearly degenerate energy levels of the $X^2\Pi$ state I_2^+. Following Hanneke *et al.* [44], we assume that a probe time equal to Γ^{-1} and minimal experimental dead time. Therefore, $\Gamma = M/\tau$, where τ is the total measurement time. We further assume that the signal-to-noise ratio $S/\delta S$ is limited by the quantum projection noise, and $S/\delta S = \sqrt{N}$, where N is the number of molecules interrogated. Therefore, the statistical uncertainty of the transition frequency is: $\delta\omega \sim \sqrt{\Gamma/\tau N}$. To estimate the sensitivity of transition frequencies, we assume that the linewidth of the forbidden transitions is on the order of 1 Hz. $\delta\alpha/\alpha$ and $\delta\mu/\mu$ that can be reached by monitoring different transitions between nearly degenerate levels of $X^2\Pi_{3/2,g}$ I_2^+ are calculated using Eq. (6) and listed in Table 3 for single-molecule detection. The sensitivities are on the order of 10^{-19} day$^{-1/2}$. The table demonstrates that $\delta\mu/\mu$ and $\delta\alpha/\alpha$ calculated using the Dirac method are close to the values obtained by substituting the fit to the experimental data [24].

The assumption of 1-second lifetimes for both energy levels used in the calculation above deserves more discussion. For a homonuclear diatomic, both pure rotational and vibrational transitions are electric-dipole forbidden. However, electric-quadruple and magnetic-dipole transitions to lower ro-vibrational levels via spontaneous emission are possible. For instance, both types of non-electric-dipole transitions within the ground ($X^3\Sigma_g^-$) state of O_2 have been reported. [45–48] Non-electric-dipole transitions between the $|X^2\Pi_{1/2,g}\rangle$ and $|X^2\Pi_{3/2,g}\rangle$ states are also possible because energy levels in these two SO substates with the same J values are coupled by S-uncoupling: [49]

Table 3
Transition frequencies (ω) between nearly degenerate energy levels of $X^2\Pi_g$ I_2^+, absolute enhancement factors ($\widetilde{K}_\mu$ and $\widetilde{K}_\alpha$), relative enhancement factors (K_μ and K_α), and corresponding sensitivities to α and μ of these transitions for single-molecule detection.

v''	v'	J''	J'	$\omega(\mathrm{cm}^{-1})$	K_μ	$\widetilde{K}_\mu$	K_α	$\widetilde{K}_\alpha$	$\delta\mu/\mu(\mathrm{day}^{-1/2})$	$\delta\alpha/\alpha(\mathrm{day}^{-1/2})$
45	17	17.5	18.5	−0.095	-4.6971×10^4	4.4622×10^3	-1.0908×10^5	1.0362×10^4	5.3487×10^{-19}	1.8126×10^{-19}
		18.5	19.5	0.086	5.1886×10^4	4.4622×10^3	1.2049×10^5	1.0362×10^4	5.3487×10^{-19}	1.8126×10^{-19}
52	23	20.5	21.5	−0.097	-5.0063×10^4	4.8561×10^3	-1.0545×10^5	1.0229×10^4	5.1496×10^{-19}	2.3185×10^{-19}
		21.5	22.5	0.105	4.6247×10^4	4.8560×10^3	9.7417×10^5	1.0229×10^4	5.1496×10^{-19}	2.3185×10^{-19}
59	29	10.5	9.5	0.348	1.5135×10^4	5.2669×10^3	2.9009×10^5	1.0095×10^4	4.5093×10^{-19}	2.3418×10^{-19}
		11.5	10.5	0.350	1.5049×10^4	5.2670×10^3	2.8843×10^5	1.0095×10^4	4.5093×10^{-19}	2.3418×10^{-19}
v''	v'	J''	J'	$\omega(\mathrm{cm}^{-1})$	K_μ	$\widetilde{K}_\mu$	K_α	$\widetilde{K}_\alpha$	$\delta\mu/\mu(\mathrm{day}^{-1/2})$	$\delta\alpha/\alpha(\mathrm{day}^{-1/2})$
30	7	18.5	19.5	0.028	8.4129×10^4	2.3556×10^3	3.5886×10^5	1.0048×10^4	1.0205×10^{-18}	2.3563×10^{-19}
		31.5	31.5	0.021	1.1218×10^5	2.3557×10^3	4.7848×10^5	1.0048×10^4	1.0205×10^{-18}	2.3563×10^{-19}
43	19	32.5	31.5	−0.092	-2.3570×10^5	2.1684×10^3	-1.0563×10^5	9.7178×10^3	1.0891×10^{-18}	2.4405×10^{-19}
		34.5	33.5	0.068	3.1891×10^5	2.1686×10^3	1.4291×10^5	9.7178×10^3	1.0890×10^{-18}	2.4405×10^{-19}
54	29	26.5	27.5	−0.069	-2.8414×10^5	1.9606×10^3	-1.3681×10^5	9.4400×10^3	1.2114×10^{-18}	2.5043×10^{-19}
		39.5	39.5	0.057	3.4433×10^5	1.9627×10^3	1.6561×10^5	9.4400×10^3	1.2101×10^{-18}	2.5043×10^{-19}
v''	v'	J''	J'	$\omega(\mathrm{cm}^{-1})$	K_μ	$\widetilde{K}_\mu$	K_α	$\widetilde{K}_\alpha$	$\delta\mu/\mu(\mathrm{day}^{-1/2})$	$\delta\alpha/\alpha(\mathrm{day}^{-1/2})$
29	6	17.5	16.5	6.604	3.6061×10^2	2.3815×10^3	1.5256×10^3	1.0075×10^4	1.0008×10^{-18}	2.3500×10^{-19}
41	17	16.5	15.5	0.483	5.5555×10^3	2.2003×10^3	2.0229×10^4	9.7708×10^3	1.0733×10^{-18}	2.4272×10^{-19}
53	28	14.5	13.5	5.651	3.5204×10^2	1.9894×10^3	1.6752×10^3	9.4665×10^3	1.1938×10^{-18}	2.5026×10^{-19}

$$\left\langle X^2\Pi_{3/2,g}, J, S=\frac{1}{2}, \sum=+\frac{1}{2} \middle| -BJ\mp S\pm \middle| X^2\Pi_{1/2}, J, S=\frac{1}{2}, \sum=-\frac{1}{2}\right\rangle = -B\left[J(J+1)-\frac{3}{4}\right]^{\frac{1}{2}} \tag{10}$$

Nevertheless, these transitions are extremely weak given their non-electric-dipole nature. In the very unlikely situation that the lifetime of either or both of the two nearly degenerate states is shorter than 1 s, the sensitivities reported in Table 3 need to be scaled by a factor of $\sqrt{\Gamma/Hz}$.

5. Conclusion

The potential energy functions of $X^2\Pi_{3/2,g}$, $X^2\Pi_{1/2,g}$, $A^2\Pi_{3/2,u}$, and $A^2\Pi_{1/2,u}$ substates of I_2^+ were obtained by high-level *ab initio* calculations. The rovibrational energy level structure and spectroscopic parameters of these states were derived using the calculated PECs and compared with the literature results. The derived spectroscopic parameters were used to reproduce a high-resolution experimental spectrum of the $A^2\Pi_{3/2,u}$ - $X^2\Pi_{3/2,g}$ system, and predict the Einstein A coefficients and lifetimes of excited states. The implications of the present work to the search for the variation of fundamental constants were discussed. We have identified nearly degenerate rovibrational level pairs in the $X^2\Pi$ state and calculated the enhancement factors for transitions between these levels.

CRediT authorship contribution statement

Yujie Zhao: Formal analysis, Methodology, Writing – original draft. **Yali Tian:** Methodology, Project administration, Writing – review & editing. **Xiaohu He:** Software, Supervision. **Ting Gong:** Investigation, Supervision. **Xiaocong Sun:** Investigation, Supervision. **Guqing Guo:** Investigation, Supervision. **Xuanbing Qiu:** Investigation, Software. **Xiang Yuan:** Methodology, Writing – review & editing. **Jinjun Liu:** Funding acquisition, Writing – review & editing. **Lunhua Deng:** Methodology, Writing – review & editing. **Chuanliang Li:** Conceptualization, Funding acquisition, Methodology, Writing – review & editing.

Declaration of competing interest

The authors declare that they have no known competing financial interests or personal relationships that could have appeared to influence the work reported in this paper.

Data availability

Data will be made available on request.

Acknowledgement

We are indebted to Prof. Wenli Zou (Northwest University, China) for his help on *ab initio*. This work was supported by the National Natural Science Foundation of China (52076145 and 12304403), the National Key Research and Development Program of China (2023YFF0718100), Fund Program for the Scientific Activities of Selected Returned Overseas Professionals in Shanxi Province (20230031), Shanxi Scholarship Council of China (2023-151), Fundamental Research Program of Shanxi Province (202303021221147 , 202203021222204 & 20230302121 2224), Taiyuan University of Science and Technology Scientific Research Initial Funding (20222121), Shanxi Province Scientific Research Initial Funding (20232033). J.L. acknowledges financial support from the NSF under Grant No. CHE-1454825.

References

[1] J. Barrow, Phil. Trans. r. Soc. a. 363 (2005) 2139–2153, https://doi.org/10.1098/rsta.2005.1634.
[2] J.-P. Uzan, Living Reviews in Relativity 14 (2011) 2.
[3] C. Chin, V. Flambaum, M. Kozlov, New J. Phys. 11 (2009) 055048. http://iopscience.iop.org/1367-2630/11/5/055048.
[4] M.G. Kozlov, S.A. Levshakov, Ann. Phys.-Berlin. 525 (2013) 452–471, https://doi.org/10.1002/andp.201300010.
[5] P. Jansen, H.L. Bethlem, W. Ubachs, J. Chem. Phys. 140 (2014) 010901, https://doi.org/10.1063/1.4853735.
[6] A. Shelkovnikov, R.J. Butcher, C. Chardonnet, A. AmyKlein, Phys. Rev. Lett. 100 (2008) 150801, https://doi.org/10.1103/PhysRevLett.100.150801.
[7] L. Pašteka, A. Borschevsky, V. Flambaum, P. Schwerdtfeger, Phys. Rev. a. 92 (2015) 012103, https://doi.org/10.1103/PhysRevA.92.012103.
[8] D. Frost, C. McDowell, D. Vroom, J. Chem. Phys. 46 (1967) 4255–4259, https://doi.org/10.1063/1.1675227.
[9] A. Cornford, D.C. Frost, C.A. McDowell, J.L. Ragle, I. Stenhouse, J. Chem. Phys. 54 (1971) 2651–2657, https://doi.org/10.1063/1.1675227.
[10] S. Evans, A. Orchard, Inorg. Chim. Acta. 5 (1971) 81–85, https://doi.org/10.1016/S0020-1693(00)95886-9.

[11] A. Potts, W. Price, Trans. Faraday, Society. 67 (1971) 1242–1252, https://doi.org/10.1039/TF9716701242.
[12] B. Higginson, D. Lloyd, P. Roberts, Chem. Phys. Lett. 19 (1973) 480–482, https://doi.org/10.1016/0009-2614(73)85130-9.
[13] H. Van Lonkhuyzen, C. De Lange, Chem. Phys. 89 (1984) 313–322, https://doi.org/10.1016/0301-0104%2884%2985319-7.
[14] R. Tuckett, E. Castellucci, M. Bonneau, G. Dujardin, S. Leach, Chem. Phys. 92 (1985) 43–57, https://doi.org/10.1016/0301-0104%2885%2980004-5.
[15] S. Mason, R. Tuckett, Chem. Phys. Lett. 160 (1989) 575–580, https://doi.org/10.1016/0301-0104%2886%2987067-7.
[16] A.J. Yencha, M.C. Cockett, J.G. Goode, R.J. Donovan, A. Hopkirk, G.C. King, Chem. Phys. Lett. 229 (1994) 347–352, https://doi.org/10.1016/0009-2614%2894%2901060-9.
[17] M. Cockett, J. Goode, K. Lawley, R. Donovan, J. Chem. Phys. 102 (1995) 5226–5234, https://doi.org/10.1016/0009-2614(93)85450-3.
[18] M.C. Cockett, J. Chem. Phys. 99 (1995) 16228–16233, https://doi.org/10.1063/1.469248.
[19] M. Cockett, R. Donovan, K. Lawley, J. Chem. Phys. 105 (1996) 3347–3360, https://doi.org/10.1063/1.472535.
[20] L.-H. Deng, Y.-Y. Zhu, C.-L. Li, Y.-Q. Chen, J. Chem. Phys. 137 (2012) 054308, https://doi.org/10.1063/1.4739466.
[21] X.-L. Mu, C.-L. Li, L.-H. Deng, H.-L. Wang, Acta Phys. Sin. 66 (2017) 233301, https://doi.org/10.7498/aps.66.233301.
[22] J. Li, K. Balasubramanian, I. Mol, Spectrosc. 138 (1989) 162–180, https://doi.org/10.1016/0022-2852(89)90108-2.
[23] W. De Jong, L. Visscher, W. Nieuwpoort, J. Chem. Phys. 107 (1997) 9046–9058, https://doi.org/10.1063/1.475194.
[24] B.R. Higginson, D.R. Lloyd, P.J. Roberts, Chemical Physics Letters 19 (1973) 480–482, https://doi.org/10.1016/0009-2614(73)85130-9.
[25] H.-J. Werner, P. J. Knowles, G. Knizia, F. R. Manby, M. Schütz, P. Celani, W. Györffy, D. Kats, T. Korona, R. Lindh, A. Mitrushenkov, G. Rauhut, K. R. Shamasundar, T. B. Adler, R. D. Amos, S. J. Bennie, A. Bernhardsson, A. Berning, D. L. Cooper, M. J. O. Deegan, A. J. Dobbyn, F. Eckert, E. Goll, C. Hampel, A. Hesselmann, G. Hetzer, T. Hrenar, G. Jansen, C. Köppl, S. J. R. Lee, Y. Liu, A. W. Lloyd, Q. Ma, R. A. Mata, A. J. May, S. J. McNicholas, W. Meyer, T. F. Miller III, M. E. Mura, A. Nicklass, D. P. O'Neill, P. Palmieri, D. Peng, K. Pflüger, R. Pitzer, M. Reiher, T. Shiozaki, H. Stoll, A. J. Stone, R. Tarroni, T. Thorsteinsson, M. Wang and M. Welborn, MOLPRO, version 2012.1, a package of ab initio programs, 2012, see.
[26] H.-J. Werner, P.J. Knowles, F.R. Manby, J.A. Black, K. Doll, A. Heßelmann, D. Kats, A. Köhn, T. Korona, D.A. Kreplin, et al., J. Chem. Phys. 152 (2020) 144107, https://doi.org/10.1063/5.0005081.
[27] K.A. Peterson, K.E. Yousaf, J. Chem. Phys. 133 (2010) 174116, https://doi.org/10.1063/1.3503659.
[28] H.-J. Werner, P.J. Knowles, J. Chem. Phys. 82 (1985) 5053–5063, https://doi.org/10.1063/1.448627.
[29] H.-J. Werner, P.J. Knowles, J. Chem. Phys. 89 (1988) 5803–5814, https://doi.org/10.1063/1.455556.
[30] A.S.P. Gomes, F. Réal, N. Galland, C. Angeli, R. Cimiraglia, V. Vallet, Phys. Chem. Chem. Phys 16 (2014) 9238–9248, https://doi.org/10.1039/C3CP55294B.
[31] S. Kervazo, F. Réal, F. Virot, A. Severo Pereira Gomes, V. Vallet, Inorg Chem 58 (2019) 14507–14521, https://doi.org/10.1021/acs.inorgchem.9b02096.
[32] X. Yuan, A.S. Pereira Gomes, J. Chem. Phys. 157 (2022) 074313, https://doi.org/10.1063/5.0092620.
[33] A. Shee, T. Saue, L. Visscher, A. Severo Pereira Gomes, J. Chem. Phys. 149 (2018) 174113, https://doi.org/10.1063/1.5053846.
[34] L. Visscher, T.J. Lee, K.G. Dyall, J. Chem. Phys. 105 (1996) 8769–8776, https://doi.org/10.1063/1.472655.
[35] DIRAC, a relativistic ab initio electronic structure program, Release DIRAC19 (2019), written by A. S. P. Gomes, T. Saue, L. Visscher, H. J. Aa. Jensen, and R. Bast, with contributions from I. A. Aucar, V. Bakken, K. G. Dyall, S. Dubillard, U. Ekström, E. Eliav, T. Enevoldsen, E. Faßhauer, T. Fleig, O. Fossgaard, L. Halbert, E. D. Hedegård, B. Heimlich–Paris, T. Helgaker, J. Henriksson, M. Iliaš, Ch. R. Jacob, S. Knecht, S. Komorovský, O. Kullie, J. K. Lærdahl, C. V. Larsen, Y. S. Lee, H. S. Nataraj, M. K. Nayak, P. Norman, G. Olejniczak, J. Olsen, J. M. H. Olsen, Y. C. Park, J. K. Pedersen, M. Pernpointner, R. di Remigio, K. Ruud, P. Sałek, B. Schimmelpfennig, B. Senjean, A. Shee, J. Sikkema, A. J. Thorvaldsen, J. hyssen, J. van Stralen, M. L. Vidal, S. Villaume, O. Visser, T. Winther, and S. Yamamoto (available at https://doi.org/10.5281/zenodo.3572669 , see also http://www.diracprogram.org).
[36] T. Saue, R. Bast, A.S.P. Gomes, H.J.A. Jensen, L. Visscher, I.A. Aucar, R. Di Remigio, K.G. Dyall, E. Eliav, E. Fasshauer, et al., J. Chem. Phys. 152 (2020) 204104, https://doi.org/10.1063/5.0004844.
[37] L. Visscher, Theor Chem Acc 98 (1997) 68–70, https://doi.org/10.1007/s002140050280.
[38] K.G. Dyall, Theor Chem Acc 117 (2007) 483–489, https://doi.org/10.1007/s00214-006-0174-5.
[39] R.J. Le Roy, J. Quant. Spectrosc. Radiat. Transfer. 186 (2017) 167–178, https://doi.org/10.1016/j.jqsrt.2016.05.028.
[40] P.F. Bernath, Spectra of atoms and molecules, Oxford University Press, 2020.
[41] C. Li, Y. Li, Z. Ji, X. Qiu, Y. Lai, J. Wei, Y. Zhao, L. Deng, Y. Chen, J. Liu, Phys. Rev. a. 97 (2018) 062501, https://doi.org/10.1103/PhysRevA.97.062501.
[42] R.J. Le Roy, J. Quant. Spectrosc. Radiat. Transfer. 186 (2017) 158–166, https://doi.org/10.1016/j.jqsrt.2016.03.030.
[43] C.M. Western, J. Quant. Spectrosc. Radiat. Transfer. 186 (2017) 221–242, https://doi.org/10.1016/j.jqsrt.2016.04.010.
[44] D. Hanneke, R. Carollo, D. Lane, Phys. Rev. a. 94 (2016) 050101, https://doi.org/10.1103/PhysRevA.94.050501.
[45] A. Goldman, J. Reid, L. Rothman, Geophys. Res. Lett. 8 (1981) 77–78, https://doi.org/10.1029/GL008i001p00077.
[46] L.S. Rothman, A. Goldman, Appl. Opt. 20 (1981) 2182–2184, https://doi.org/10.1364/AO.20.002182.
[47] A. Goldman, C. Rinsland, B. Canova, R. Zander, M. DangNhu, J. Quant. Spectrosc. Radiat. Transfer. 54 (1995) 757–765, https://doi.org/10.1016/0022-4073(95)00114-Z.
[48] L.R. Zink, M. Mizushima, J. Mol. Spectrosc. 125 (1987) 154–158, https://doi.org/10.1016/0022-2852(87)90201-3.
[49] H. Lefebvre-Brion, R.W. Field, The Spectra and Dynamics of Diatomic Molecules, Elsevier Academic Press, 2004.